Estimation of Distribution Algorithm (EDA) for Design and Optimization of Arch Structures

Bioresource Technology 396 (2024) 130446

Contents lists available at ScienceDirect

Bioresource Technology

journal homepage: www.elsevier.com/locate/biortech

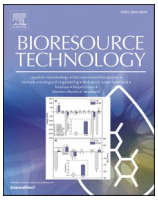

Understanding the effect of heating rate on hydrothermal liquefaction: A comprehensive investigation from model compounds to a real food waste

Edoardo Tito, Carlo Alberto Marcolongo, Giuseppe Pipitone *, Alessandro H.A. Monteverde, Samir Bensaid, Raffaele Pirone

Department of Applied Science and Technology, Politecnico di Torino, Corso Duca degli Abruzzi 24, 10129 Turin, Italy

HIGHLIGHTS

- Different heating rates were tested in HTL of model compounds and real food waste.
- Heating rate strongly affected HTL performances at lower residence times.
- Heating rate influence at longer residence times was limited.
- HTL performance was well described by the kinetic severity factor.

GRAPHICAL ABSTRACT

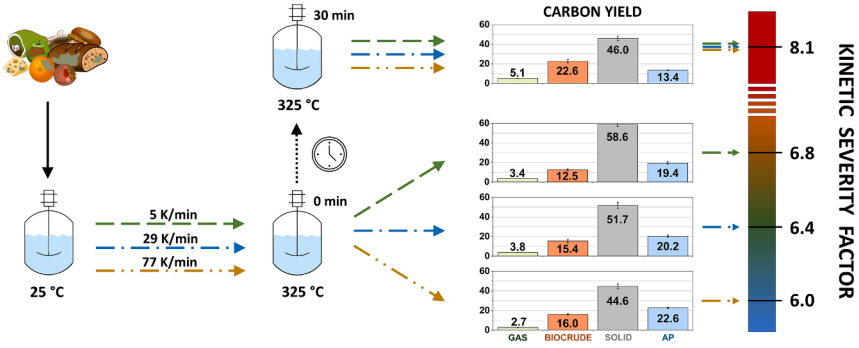

ARTICLE INFO

Keywords:
Food waste
Heating rate
Biocrude
Fast hydrothermal liquefaction
Kinetic severity factor

ABSTRACT

Hydrothermal liquefaction (HTL) emerges as an efficient technology for converting food waste into biocrude. Among HTL parameters, the impact of heating rate is understudied. This study systematically explores its variation (5–115 K/min) on HTL performance using actual food waste and model compounds representing its constituents. Results revealed that an increase in heating rates significantly impacts HTL performances (+63 % biocrude and −34 % solid with food waste) with short residence times, as slower heating rates imply a longer overall time and a higher kinetic advancement of the reaction. Conversely, with longer residence times, the influence of heating rates becomes negligible, as kinetics during heating times are overshadowed by those at operating temperatures. A subtle effect of heating variation at extended residence time was observed only with carbohydrates. This research emphasizes the utility of a kinetic severity factor (KSF) as a valuable tool for simultaneously considering heating rates, operating times, and temperatures.

1. Introduction

Nowadays, the quest for sustainable energy sources is more important than ever. The CO_2 level in the atmosphere is rising relentlessly, and the use of fossil fuels, which is its main cause, is facing increasing resistance. Beyond environmental concerns, the transition

* Corresponding author.
E-mail address: giuseppe.pipitone@polito.it (G. Pipitone).

https://doi.org/10.1016/j.biortech.2024.130446
Received 13 December 2023; Received in revised form 30 January 2024; Accepted 9 February 2024
Available online 15 February 2024

away from fossil fuels should be pursued due to their finite nature and the geopolitical tensions they entail. A possible solution to these problems is bioenergy obtained from biomass. Biomass is renewable because it is regenerated in biogenic cycles comparable to human use and is evenly globally distributed. Among the various types of biomasses that could be exploited (algae, energy crops, wood residues, sludges, etc.), the exploitation of food waste is particularly interesting. Food waste is produced in large quantities, especially in areas with high residential density where energy demand is higher, and it is considered a waste that needs to be disposed of. Approximately one-third of the world's edible food is wasted, amounting to 1.3 billion tons of organic material, with nearly half of it occurring after the post-harvest stage and before retail (FAO, 2019, 2011).

While the potential for significantly reducing inefficiencies and losses along the supply chain exists, the generation of food waste remains inevitable, necessitating the imperative to address its management. Currently, the most common solution used worldwide is landfilling, which leads to release of harmful GHGs, followed by incineration (FAO, 2013). The latter allows for the recovery of some energy in the form of electricity and thermal energy, following the waste-to-energy concept. However, due to the high moisture content of food waste, it has low efficiency. Several other technologies could be used for biomass energetic valorization and, among these, hydrothermal liquefaction (HTL) stands out as a promising thermochemical process capable of converting organic waste into valuable biocrude and other useful products through reaction with water at high temperature and pressure (250–400 °C, 50–250 bar) (Kumar, 2022). Taking place in a hydrothermal environment, HTL is particularly suitable for wet feedstock, which would otherwise require energy-intensive drying processes before valorization through dry technologies (like pyrolysis), resulting in lower overall energy efficiency. The interest in HTL of food waste is consequently growing (Chen et al., 2020; Motavaf and Savage, 2021).

The HTL reaction is known to be influenced by various operating parameters, with the order of importance being: nature of the feedstock, temperature, residence time, solid loading and pressure (Fan et al., 2023; Mishra et al., 2022). Although a lot is known about the influence of the aforementioned parameters, little is still understood about the effect of heating rate on HTL performance (Fan et al., 2023; Mathanker et al., 2021). Moreover, to the best of the authors' knowledge, the very few studies available have solely focused on the effect of heating rate on lignocellulosic feedstocks and, no studies on food waste have been performed. However, this is a key gap, since the biochemical composition of the feedstock strongly influences the reaction pathways, as extensively documented (Déniel et al., 2017; Yang et al., 2019).

According to the few studies on lignocellulosic feedstock, usually higher heating rates lead to an increase in the conversion of the feedstock and the production of biocrude. Brand et al. tested HTL of pine sawdust at temperatures ranging from 250 to 350 °C with two different heating rates: 2 and 20 K/min (Brand et al., 2014). They observed increased solid conversion and biocrude yield as the heating rate increased, particularly at reaction temperatures higher than 280 °C and with a residence time of 1 min. Bach et al. also confirmed the positive effects on biocrude yield when increasing the heating rate from 136 K/min to 585 K/min, after testing a macroalga at 350 °C for 15 min (Bach et al., 2014). Similarly, Tran et al. also observed increased biocrude production at the expenses of solids and aqueous-solubles when they increased the heating rate from 66 to 169 K/min during HTL of wood at 350 °C for 15 min (Tran et al., 2017). However, the 15-minute duration included the heating time, so lower heating rates resulted in a shorter effective reaction time.

Except for the study on cellulose by Kamio et al. (Kamio et al., 2008), all the aforementioned studies used real biomass as feedstock. While the use of real biomass enables the direct observation of how the heating rate affects the actual implementation of the HTL, a more in-depth understanding of the chemical mechanisms leading to variations in performance could be achieved by employing model compounds. Hence, this would enable to generalize the obtained results to all types of biomass. Furthermore, focusing only on short residence times, it is impossible distinguishing between a direct influence of the heating rate, linked to variations in chemical pathways during the heating period, and any indirect effects, associated with a different kinetic advancement of the reaction. In recent years, the use of the fast HTL has gained interest as an alternative to isothermal HTL (Faeth et al., 2013; Hietala et al., 2016; Qian et al., 2020). The former requires very fast heating rates (from 100 K/min to 100 K/s), high set-point temperatures (up to 600 °C), and limited residence times (less than 1 min) (Faeth et al., 2013; Qian et al., 2020). This is in contrast to isothermal HTL, which involves longer residence times (>15 min) at lower temperatures (250–350 °C) (Mathanker et al., 2021). Because these two techniques have significantly different residence times, the effect of the heating rate can have varied implications in each case.

This work aims to address this knowledge gap by systematically investigating the effect of heating rate on HTL of food waste. Real food waste from the university canteen was used as feedstock, as well as monomer compounds - cellulose, albumin, and triolein – chosen to mimic the essential components representing carbohydrates, proteins, and lipids, respectively. This approach enabled us to investigate how varying heating rates affect both real biomass and its constituent parts, thereby enhancing the comprehension of the chemistry involved during the HTL reaction. Experiments were conducted for each feedstock by keeping all operating parameters fixed while varying only the heating rates and reaction times to exclude other influences. Additionally, to improve the understanding of any kinetic implications arising from the varied heating rates employed, a kinetic severity factor was utilized.

2. Materials and methods

2.1. Materials

Cellulose (microcrystalline powder, Sigma-Aldrich) was used as the representative of carbohydrates, as typically reported (Changi et al., 2015; Mahadevan Subramanya and Savage, 2021). Albumin from egg white (powder, 62–88 %, Sigma-Aldrich) was used as the protein representative, as commonly done (Biller and Ross, 2011; Teri et al., 2014). The batch used had a purity of 75 %, with the remaining portion consisting of other proteins, namely conalbumin (10–15 %), ovomucoid (10–15 %), lysozyme (~2%), globulin, ovomucin and avidin. As for the lipid representative, glyceryl trioleate (~65 %, Sigma-Aldrich), also known as triolein, was chosen, despite the common usage of vegetable oils like soybean, rapeseed, and sunflower oil (Changi et al., 2015). However, these oils are not composed solely of triglycerides, and the fatty acids by which they are composed of are different. To achieve higher feed purity, glyceryl trioleate was employed. The batch used was entirely composed of triglycerides, with 88 % of its fatty acids constituents being oleic acid, while the remaining portion consisted of palmitic and linoleic acid. Polymers, instead of monomers, were selected as model compounds to integrate the hydrolysis step into the analysis.

Food waste was collected from the university canteen after service, blended for homogenization and then stored in a refrigerator until needed for the reaction.

2.2. Reaction and work-up

Experiments were conducted using bomb-type batch reactors with an internal volume of 20 ml (Fig. S1-A). The reactors were assembled by closing off one end of a 316 stainless steel tube using a 3/4″ cap. At the opposite end, a 3/4″-1/4″ reducing union was positioned, with a 1/4″ cap affixed to a 1-inch-long 1/4″ tube. A slightly different reactor configuration was used to assess the gas composition. A 1/4″-1/8″ reducing union was attached to one end of the 3/4″-1/4″ reducing union, and a 50 cm-long 1/8″ stainless steel tube was connected to it. This tube was sealed with a screwed bonnet needle valve, as pictured in Fig. S1-B. All

fittings used were FITOK® and made of stainless steel.

Prior to reaction, the reactor was loaded with 1.8 g of dry feedstock and distilled water to achieve a total mass of 9 g. In the case of food waste, all experiments were performed within 11 days to avoid variations in moisture content. After loading, the reactor was then submerged into a sand bath (Techne© SBL-2D) equipped with a temperature controller (Techne© TC-9D). Four different heating rates were tested, and the submersion of the reactor was performed differently for each, as described in Paragraph 2.3. The operating temperature for all reactions was 325 °C, while two reaction times were used: 0 and 30 min. The 30-minute test was not performed for the highest heating rate used in this work. After reaction, the reactor was removed from the sand bath and quenched in water at ambient temperature. Within less than 30 s, the internal temperature dropped below 50 °C. The reactor was left in water for further 5 min.

After washing and drying with compressed air, the reactor was weighed. It was then opened to vent the produced gas, and weighed again. The difference in weight gave the mass of gas produced. The content of the reactor was poured into a 50 ml centrifuge tube. Diethyl ether (DEE) was used to rinse the reactor and remove any possible solid and oil residues, along with mechanical action using a spatula. At least 36 ml of DEE were used, subdivided into multiple aliquots. If the cleaning solvent was not transparent, additional DEE was added until transparency was achieved. All the DEE used was added to the 50 ml centrifuge tube containing all the produced phases. The centrifuge tube was then shaken and placed in a vibro-mixer to ensure thorough mixing of all phases present. Subsequently, the tube was inserted into a centrifuge and spun for 8–10 min at 4500 rpm to fasten phase separation and solid sedimentation.

The lightest apolar phase, which contained the biocrude, was collected using a Pasteur pipette and vacuum-filtered through a qualitative filter paper (Whatman grade 5). The resulting polar phase was then dried with sodium sulfate and evaporated in a rotary evaporator. The resulting biocrude was then weighed and stored for subsequent analysis.

The aqueous phase (AP) was vacuum-filtered using the same filter employed for the apolar phase. Attention was paid to ensuring that all the solid in the tube was transferred onto the filter. Subsequently, the AP was then left for 36 h under a chemical hood to remove any residual DEE and then stored. The solid-containing filter was left overnight in oven at 105 °C to remove any residual moisture; it was then weighted and the solid collected. The mass yields of the different phases were determined by dividing their dry mass by that of the feedstock loaded into the reactor. The mass yield of the AP was calculated as the difference between 100 % and the sum of the mass yields of solid, gas and biocrude. However, a more precise quantification of the amount of AP-solubles was performed using the carbon yield, as reported in Paragraph 2.4.

Blank tests were conducted with each feedstock to analyze their solubilities. The blanks were prepared by mixing each feedstock with an amount of water equal to that used in the reactions. Then, the previously described work-up was performed without conducting the reactions beforehand. The results are reported in Table S1. All reactions at 0 min were performed at least on duplicate, while reactions at 30 min were performed at least on triplicate. Carbon balance resulted always higher than 77 %.

2.3. Heating rates

The experiments employed four heating rates. Different procedures were followed to obtain these rates:

- 5.2 K/min: the reactor was immersed in a sand bath at ambient temperature, operating in the bubbling fluidization regime. After immersion, the set-point temperature of the sand bath was raised to 325 °C. During the sand bath's heating process, the air's fluidization flow rate was adjusted to maintain the bubbling fluidization regime and prevent sand spillage;
- 29 K/min: the reactor was submerged into the sand bath while stable at the set-point temperature of 325 °C and within the bubbling fluidization regime. Immediately after submersion, the airflow for fluidization was halted, reducing the heat exchange coefficient. After 3 min, the sand bath was brought to the minimal fluidization velocity for 3 min long; after that the sand bath was returned to the bubbling fluidization regime;
- 77 K/min: the reactor was submerged into the sand bath while stable at the set-point temperature of 325 °C and within the bubbling fluidization regime;
- 115 K/min: the reactor was submerged into the sand bath while stable at a temperature of 360 °C and within the bubbling fluidization regime. This heating rate was exclusively used for a residence time of 0 min.

The heating rates were evaluated by using proxy reactors filled with 9 g of water and fitted with a 1/16″ type K thermocouple, which enabled the plotting of the internal temperature over time. Heating rates were then calculated as the time required to reach 95 % of the overall temperature change (Hietala et al., 2016). Accordingly, to reach 325 °C from the initial 25 °C, the heating rate was estimated based on the time needed to reach 310 °C. Fig. S2 presents the temperature profiles for the different cases, while the evaluated heating rate are reported in Table 1. Reactions conducted at 0 min were quenched upon reaching 310 °C, while reactions at 30 min were stopped 30 min after reaching 310 °C.

Variations in HTL performance resulting from modifications in heating rate could be attributed to two causes. An 'indirect' cause is associated with higher or lower kinetic advancement of the reaction due to the fact that a slower/faster heating rate leads to longer/shorter heating times. On the other hand, another ('direct') cause could result from the fact that remaining at lower temperatures during the heating phase could lead to changes in the chemical mechanisms and formation pathways of the different phases. Indeed, reactions at lower temperatures typically result in increased production of the solid phase (hence it is indeed called 'hydrothermal carbonization' rather than 'hydrothermal liquefaction') (Mathimani and Mallick, 2019), and prolonged exposure to lower temperatures could lead to irreversible formation of solid. To distinguish between these two causes, the kinetic severity factor (KSF, Eq. (1) was used in this study. T(t) denotes the temperature (°C) at time t (min); t_0 corresponds to the starting time, while t_f represents the ending time of the reaction.

$$KSF = log_{10}(R^0) = log_{10}\left(\int_{t_0}^{t_f} e^{\frac{T_{(t)}-100}{14.75}} dt\right) \quad (1)$$

The kinetic severity factor was initially employed by Overend and Chornet to account for both the effects of temperature and reaction time during aqueous/stream pretreatments of lignocellulosic biomasses, expressing the severity through a single factor (Overend and Chornet, 1987). The KSF was derived from a first-order kinetic model, assuming a constant of 14.75 K, experimentally derived, and a reference temperature of 100 °C (Chum et al., 1990). Currently, the KSF is widely applied in the study of HTL (Castello et al., 2018; Cheng et al., 2018; Faeth et al., 2013; Prestigiacomo et al., 2020; Ruiz et al., 2013), as it is considered a reliable method for describing the kinetic severity of the process. Moreover, Prestigiacomo et al. recently observed that the KSF can be efficiently used as parameter to estimate the HTL performance

Table 1
Heating rates and kinetic severity factor for all the different cases.

Heating rate (K/min)	5.2	29	77	115
KSF at 0 min	6.8	6.4	6.0	5.7
KSF at 30 min	8.1	8.1	8.1	–

(Prestigiacomo et al., 2022).

The KSF was calculated for all the performed tests. As shown in Table 1, increasing the heating rate at 0 min leads to a decrease in kinetic severity, while alterations in the heating rate at 30 min do not affect it. The difference arises because, at 0 min, the entire residence time is dedicated to heating, leading to a more significant reaction advancement for lower heating rates. In contrast, at 30 min, the impact of heating time is negligible, as the reaction kinetics at the setpoint temperature dominate. Therefore, variations in heating rates at 30 min are crucial for confirming or refuting a 'direct' effect on HTL, while differences at time 0 only offer an indication of the reaction's progression.

2.4. Analysis

To asses the gas composition, experiments at 30 min were performed with the reactor configuration explained above. Before the reaction, the reactor was loaded and then purged and pressurized with 9 bars of He. The resulting gas phase was then sampled and examined using a Micro-GC (SRA) equipped with Molsieve 5A and PoraPLOT U columns, along with a TCD detector. The average composition obtained at 30 min with the three different heating rates was used to evaluate the carbon content of the gas for all the tests at both 0 and 30 min.

An elemental analyzer (Elementar vario Macro Cube) was used to determine the elemental composition (CHNS) of feedstocks, solids, aqueous phases and biocrudes. Only samples of at least 20 mg were analyzed, each at least in triplicates. Carbon and nitrogen yields were calculated by dividing the masses of carbon and nitrogen in the products by the carbon and nitrogen content of the feedstock. For quantifying aqueous-soluble compounds, HPLC (Shimadzu) was used. 10 µl of aqueous sample was injected in a Rezex ROA-Organic acid H + (8 %) column (300 mm · 7.8 mm) at a thermostat temperature of 50 °C, using a mobile phase of 5 mM H_2SO_4 and a flow rate of 0.7 ml/min.

To determine the compositions of the biocrudes, a GC–MS (Agilent 7890B GC-Agilent 5977A) was employed. A volume of 0.9 ml of biocrude solution in acetone (ca. 10 mg/ml) was subjected to derivatization with 0.1 ml of BSTFA (+1% TCMS) for 1 h in a glass vial while being stirred over a magnetic plate at 70 °C. The derivatized sample was then injected in a DB-5 ms column (dimensions 30 m × 0.25 mm × 25 µm) using a split ratio of 20:1 and an injection temperature of 280 °C. The helium flow in the column was kept constant at 1 ml/min, and the temperature was programmed as follows: 40 °C (5 min soak) // 10 °C/min // 100 °C (0 min soak) // 4 °C/min // 280 °C (0 min soak)// 10 °C/min // 300 °C (0 min soak). Compound identification was carried out using the NIST 17 library and the subdivision between the different types of molecules was based on their functionalities. In the case of molecules containing more than one functionality, their identification was assigned based on the following priority order: S-containing molecules > DKPs > N-containing aromatics > imines/nitriles > cyclic amides/cyclic imides > amides > amines > long fatty esters > monoglycerides > long fatty acids > PAHs > O-containing aromatic rings > phenols > benzenes > furans > acid > oxygenated. In the case of biocrudes obtained from albumin at 0 min, the biocrude samples were injected into the GC–MS without prior derivatization. This was necessary due to the NIST library's inability to identify most of the derivatized peaks.

To assess the biochemical content of the food waste, lipids, proteins and ashes were measured, while carbohydrates were calculated by difference. The protein content was calculated by multiplying the nitrogen content, which was evaluated through elemental analysis, by a factor of 6.25 (Simonne et al., 1997). For lipid content determination, the biomass was dried overnight in an oven at 105 °C. Subsequently, 7 g of dry biomass were subjected to extraction using a Soxhlet extractor with 200 ml of petroleum ether heated to 70 °C for 6 h. The extracted material was then subjected to evaporation by rotary evaporator to remove the petroleum ether, and the remaining mass was accounted for as lipids. The ashes of the feedstock were measured by combustion at 550 °C for 3 h in an oven. Alternatively, the ashes of the produced solids were measured via thermogravimetric analysis (TGA, Mettler Toledo SDTA851) with the following temperature program: 25 °C (0 min soak) // 30 °C/min // 900 °C (10 min soak) under an airflow of 50 ml/min.

3. Results and discussion

3.1. Cellulose

Fig. 1 depicts the mass yields obtained after HTL of cellulose. With the exception of the compounds soluble in the AP (not reported), the most abundant phase is the solid one, as typically observed from carbohydrates (Biller and Ross, 2011; Teri et al., 2014). However, despite being completely insoluble in water (Table S1), cellulose yielded only 18 % as a solid at 0 min and 115 K/min. The mass yield of glucose was 21 % at 115 K/min, 2 % at 77 K/min and zero for lower heating rates. Cellulose hydrolysis takes place in few seconds in hydrothermal environment (Sasaki et al., 1998) and the heating time was likely long enough to allow for glucose formation and its further conversion.

At 0 min, with decreasing heating rate, the amount of solid produced continuously increased. AP-soluble compounds formed from cellulose, in particular furanic compounds, are prone to repolymerization into solid humins (Rasmussen et al., 2014). Their formation is likely kinetically limited, and the increase in KSF with lower heating rate could explain the increase in solid. After 30 min at set-point temperature, the differences between the heating rates became less pronounced, despite the same trend was still visible: the solid yield at higher heating rates increased, as humins did not have enough time to be formed during the heating time, while at the lowest heating rate slightly decreased, likely due to a partial degradation of the excessively formed solid.

An increasing yield with decreasing heating rate was also observed for the gas phase at 0 min, as expected since gaseous compounds are end-products (Gollakota et al., 2018). A higher extent of the reaction would result in their increased production, as observed after further 30 min. At 30 min the gas phase was composed by CO_2 (80–83 vol%) and CO (15–18 vol%).

Biocrude production showed an opposite trend. Biocrude-forming compounds are hence likely formed directly from cellulose degradation and are intermediate in the formation of other compounds, as confirmed also by the slight decrease in yield after 30 min of reactions. This aspect will be deepened by GC–MS analysis reported below.

The elemental compositions of solids and biocrudes are reported in

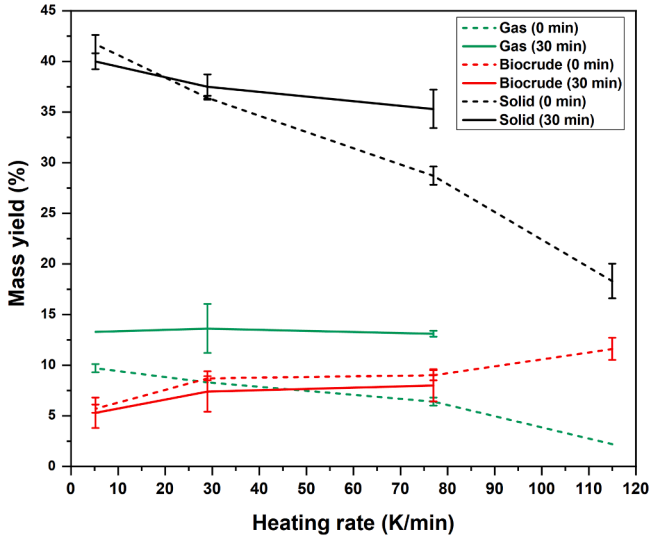

Fig. 1. Mass yields obtained from cellulose. Reaction conditions: 1.8 g cellulose, 9 g total, 325 °C, 0 and 30 min.

Fig. 2-A. After the reaction, the elemental composition of the solid drastically changed from cellulose, with carbon increasing significantly at the expense of oxygen. However, except at 115 K/min run and 0 min, the elemental composition of the solid did not change significantly with different heating rates. Additionally, an increase in the reaction time did not significantly affect the solid composition. Therefore, it is likely that the solid observed after reaction at 0 min and 115 K/min was actually a mixture of unconverted cellulose and solid product. That run, in fact, lasted just the few minutes necessary for heating, and it is probable that cellulose hydrolysis was not completed. However, already at 0 min and 77 K/min the elemental composition was the same observed in all the other runs. Despite minimal changes in the elemental composition, the carbon yield in the solid (Fig. 2-C) strongly increased with lower heating rates at 0 min. Hence, solid humins are formed by the condensation of compounds soluble in the AP within a time frame comparable to the heating duration.

At 0 min, the biocrude elemental composition (Fig. 2-B) mostly showed an increase in hydrogen content with decreasing heating rate. After 30 min, the carbon content slightly increased, while oxygen and hydrogen decreased. However, no differences were registered between the different heating rates. The breakdown of compounds present in the biocrudes is depicted in Fig. 2-D, while the most prevalent compounds are listed in Table S2. At low KSFs, a consistent amount of furanic molecules and oxygenates were identified. In particular, the former are known to be prone to polymerize into solid humins (Tito et al., 2023a; Velasco Calderón et al., 2022), thus explaining the opposite trends of furanic compounds and biocrude yield in relation to solid formation. Despite solid formation cannot be explained solely by the conversion of biocrude-soluble compounds, as the biocrude content remained low under all conditions, the presence of these compounds in the biocrude is indicative of similar compounds in the AP, as their polarity and solubility are intermediate (Jakob et al., 2021). With increased KSF, the amount of acids and phenols increased. Phenolic compounds are known to be the final product during HTL of saccharides (Toor et al., 2011) and levulinic acid, identified as the most prevalent acid, results from dehydration of 5-HMF, which was also identified in the AP through HPLC.

As for the mass yield, the majority of the carbon yield was directed towards the solid phase (Fig. 2-C). At 30 min, a slight effect of the heating rate was observed, with solid favored and biocrude disfavored at lower heating rates. The AP carbon yield was consistent at low KSF due to hydrolysis of cellulose into glucose and subsequent formation of oxygenated intermediates that subsequently converted into solid.

Overall, after 0 min of reaction, the heating rate is shown to have a strong effect on the HTL of cellulose, both quantitatively and qualitatively. At higher heating rates, the heating time is not sufficient to complete the conversion of furans and aqueous-soluble compounds into solid humins, aromatics, and levulinic acid. Conversely, after 30 min of reaction, the heating rate appears to have a minor impact on mass yields, favoring a slightly higher biocrude yield over solid yield at elevated heating rates. This could be attributed to humins formation occurring at low temperatures (Tito et al., 2023a), and thus, a shorter stay at lower temperatures during the heating time limits the amount of solid formed. On the other hand, from a qualitative perspective, the differences at 30 min were almost negligible.

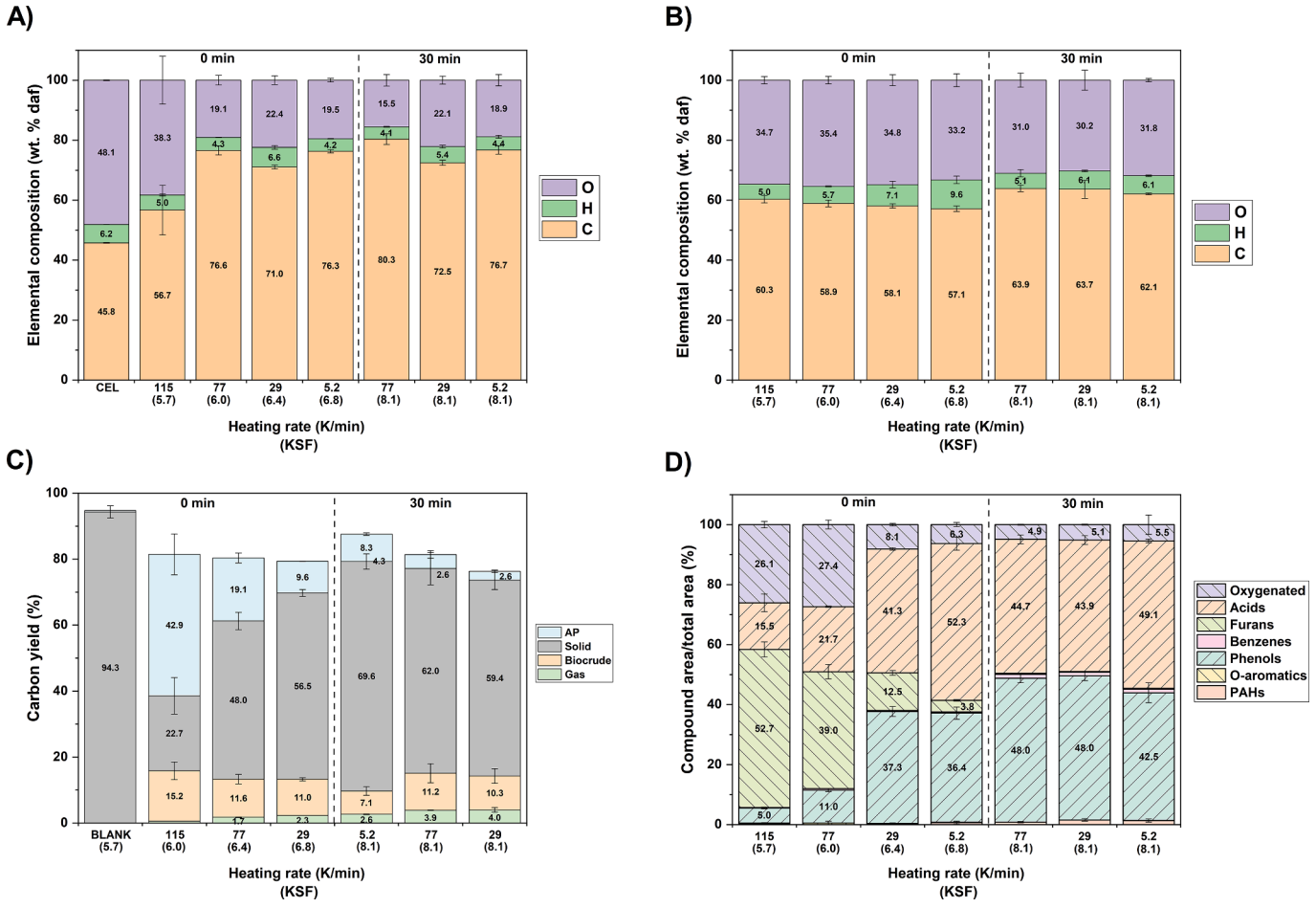

Fig. 2. (A) Elemental composition of solids and feedstock (CEL); (B) elemental composition of biocrudes; (C) carbon yields of all the phases; (D) families of compounds identified in the biocrudes by GC–MS. Data refer to products obtained from cellulose at 325 °C with different heating rates and with two residence times (0 min, 30 min).

3.2. Albumin

Fig. 3 depicts the mass yields obtained after HTL of albumin. 88 % of albumin is soluble in the AP at room temperature (Table S1), and after every reaction, the AP yield was within 64–74 % (not reported). Hence, the fraction of albumin soluble in the AP was converted into the other phases. At 0 min, the solid phase decreased with a decreasing heating rate, hence increasing KSF, in contrast to what happened with cellulose. However, at 77 K/min and above, the solid yield was consistently higher than the solid fraction of albumin. As already observed after fast HTL of bovine serum albumin (Sheehan and Savage, 2017), above 78–86 °C ovalbumin is denatured into a more stable and hydrophobic structure that results in an increased solid yield (Chay Pak Ting et al., 2013). With increasing KSF, the denatured structure is then slowly converted, resulting in a 4.7 % of solid yield. After further 30 min at 325 °C, the solid phase further decreased up to 1.4–1.9 %, likely attributable to the ashes present in albumin, as 6 % of the albumin constituted ash (Table S1).

Biocrude increased with a decreasing heating rate at 0 min and further increased after 30 min at 325 °C. This increase implies the occurrence of secondary reactions contributing to biocrude production. One possible explanation for this phenomenon is the conversion of the solid phase into biocrude, as indicated by the opposing trends observed between the two phases. During HTL, proteins are hydrolyzed to smaller peptides with a decreasing molecular weight as the residence time increases (Aida et al., 2017). Most of the degradation products of peptides are amines and AP-solubles (Sheehan and Savage, 2017). HTL experiments with amino acids showed a limited biocrude production (Dote et al., 1998; Tito et al., 2023a), hence suggesting that biocrude production takes place directly from the degradation of the solid polypeptides. As observed with cellulose, gas yield increased with decreasing heating rate at 0 min and increased after further 30 min, confirming the increased production as KSF increases. At 30 min, 96–98 vol% of the gas phase was composed by CO_2.

The elemental composition of the solids and biocrudes is depicted in Fig. 4-A/B. In addition to carbon, hydrogen and oxygen, albumin contains a noteworthy amount of nitrogen and a small sulfur fraction, leading to the classic sulfur odor after the HTL reaction. The solid fraction of unconverted albumin exhibited lower oxygen levels compared to the overall albumin composition, and following a reaction at 0 min, the oxygen content in the residual solid further decreased. However, decreasing the heating rate, and consequently increasing the KSF, the elemental composition of the solid did not change significantly.

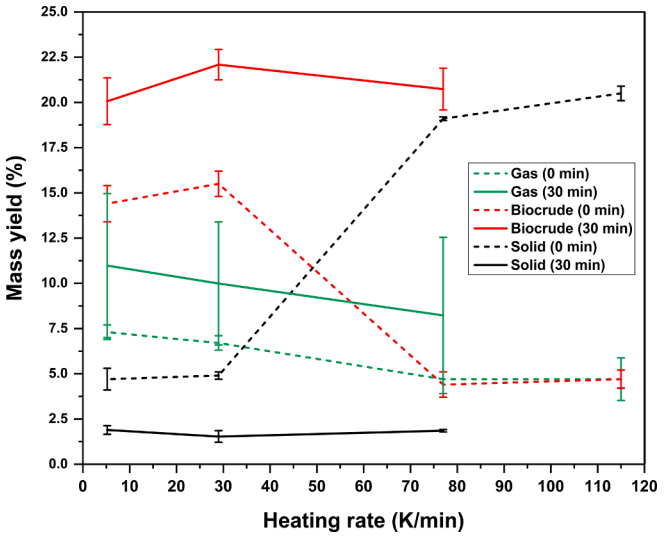

Fig. 3. Mass yields obtained from albumin. Reaction conditions: 1.8 g albumin, 9 g total, 325 °C, 0 and 30 min.

It is hence possible that degradation of the albumin solid phase may occur through a random scission mechanism that does not occur on precise portions of molecules, as speculated by Aida et al. (Aida et al., 2017), until complete conversion.

Regarding the biocrudes (Fig. 4-B), it was not possible to obtain the elemental composition at high heating rates at 0 min due to their low mass yields, which made it difficult to identify a trend. However, by increasing the reaction time from 0 to 30 min, carbon and hydrogen increased at the expenses of oxygen and nitrogen. That is an interesting result that confirms that with longer residence times, the amount of heteroatoms in the biocrude decreases, providing a higher-quality product that can be more easily upgraded to biofuel.

The molecular compositions of biocrudes are reported in Fig. 4-E/F, while the highest identified peaks are reported in Tables S3-S4. It is worth noting that the results of Fig. 4-E and Fig. 4-F are not directly comparable due to the different derivatization method used, as explained in the Materials and Methods section. At 0 min most of the compounds identified by GC–MS were amides (amides, cyclic amides/imides and diketopiperazines), which accounted for 60–72 % of the overall area (Fig. 4-E). Among these, the most abundant molecules were diketopiperazines (DKPs) derivatives, which are associated with hydrolysis of proteins. DKPs were observed to be formed through cyclization of amino acids (Sakata et al., 2010; Zhang et al., 2016) and were inferred to be hydrolysis products resulting from progressive cyclization, forming smaller and smaller cyclic peptides until they became DKPs (Torri et al., 2012). As the heating rate decreased, the relative area of DKPs decreased in favor of other amides (cyclic amides/imides and linear amides), suggesting that their formation occurred through degradation of DKPs (Zhang et al., 2016). With decreasing heating rate even the nitrogen-containing aromatics increased, with indole derivatives being the most abundant, along with benzenes and phenols. Indoles are likely the result of interactions between phenols and amino acids (Madsen et al., 2017), while phenols and benzenes could be produced by interactions and recombination of oxygenated molecules (Déniel et al., 2016; Qiu et al., 2019).

After 30 min of reaction time, the differences at various heating rates were negligible (Fig. 4-F). Most of the identified molecules were amides, followed by aromatics (phenols, nitrogen-containing and benzenes) and amines. Among the nitrogen-containing aromatics, indoles were the most present ones. Amines are formed after complete hydrolysis of proteins into amino acids, and residual amino groups can persist after recombination of amino acids into other molecules. In fact, many of the amines identified in this work also contained other functional groups, primarily aromatic rings. Finally, the presence of sulfur-containing molecules was very limited after both 0 and 30 min of reaction time.

The carbon distribution among the different phases (Fig. 4-C) confirmed the observations made based on the mass yields (Fig. 3). Specifically, it revealed a decrease in the solid phase and an increase in biocrude with the increasing KSF. Moreover, Fig. 4-C provides confirmation that, prior to the reaction, most of the carbon in the albumin feedstock was present in the AP. During the heating time, a portion of the AP-soluble fraction became entrapped in the solid phase due to the denaturation. In addition to this, another portion of the AP-solubles was converted into the biocrude phase.

As for the nitrogen distribution (Fig. 4-D), the trends closely resembled those observed for carbon distribution. However, compared to the carbon yields, the nitrogen yields in both the solid and biocrudes were significantly lower, with a preference for the AP. This was expected as nitrogen is more polar than carbon, and nitrogen-containing functional groups tend to have higher aqueous solubility.

Overall, as observed with cellulose, the heating rate strongly affects the HTL performance of albumin, both quantitatively and qualitatively, at 0 min. However, after 30 min of reaction time, the effects of heating rate were not observable.

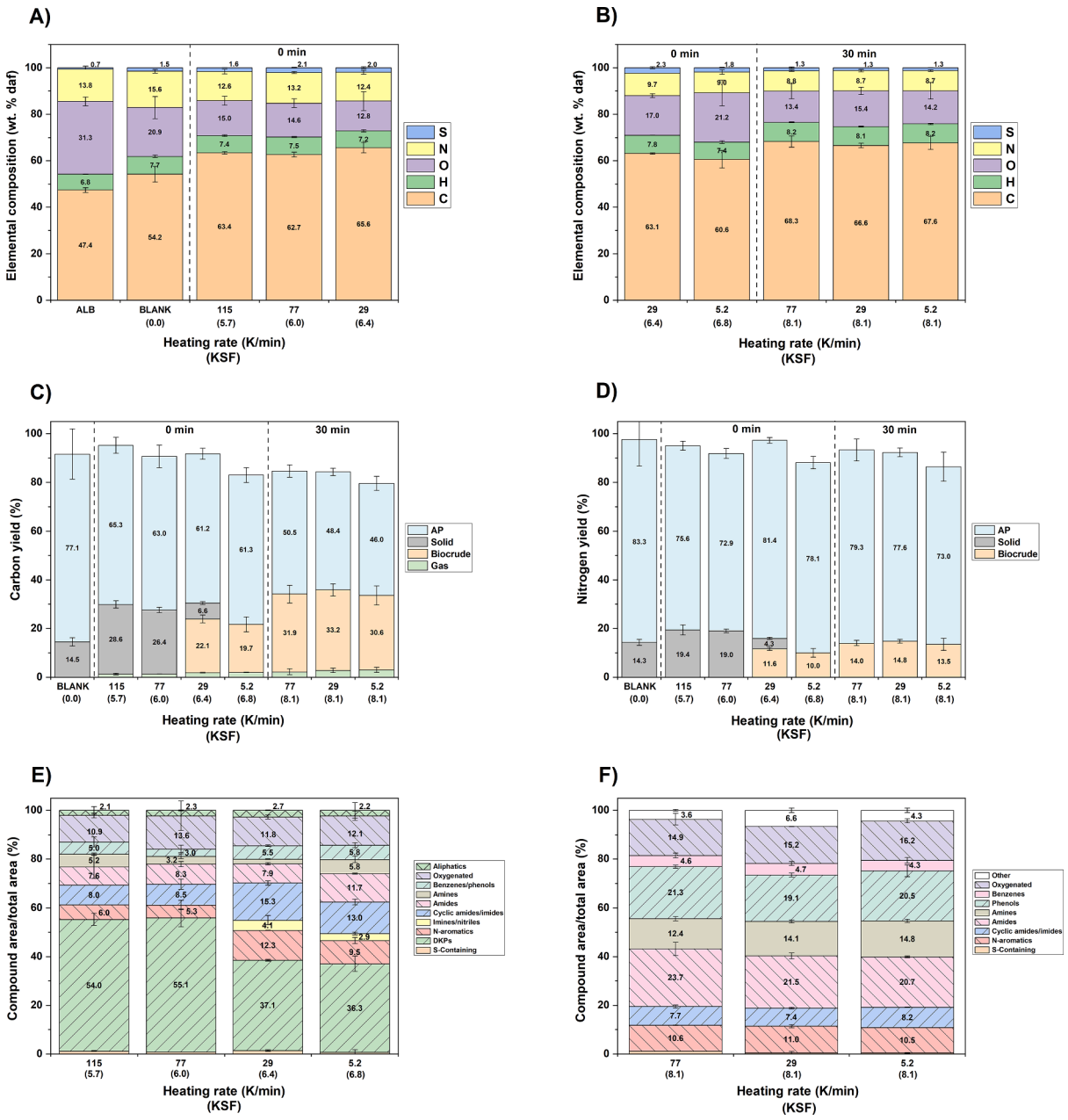

Fig. 4. (A) Elemental composition of solids, feedstock (ALB) and its solid fraction (BLANK); (B) elemental composition of biocrudes; (C) carbon yields of all the phases; (D) nitrogen yields of all the phases; (E) families of compounds identified in the biocrudes obtained at 0 min by GC–MS without derivatization with BSTFA; (F) families of compounds identified in the biocrudes obtained at 30 min by GC–MS after derivatization with BSTFA. Data refer to products obtained from albumin at 325 °C with different heating rates and with two residence times (0 min, 30 min).

3.3. Triolein

During HTL of triglycerides, the oil phase is the predominant product, as depicted in Fig. S3. This is due to the fact that triglycerides are insoluble in the AP, and the main reaction they undergo is hydrolysis (Changi et al., 2015), resulting in the formation of free fatty acids, which remain insoluble in the AP, and glycerol, which is soluble in water. Stoichiometrically, complete hydrolysis of triolein would yield 95.7 % as biocrude and 10.4 % as AP (due to glycerol) on a mass base. The average biocrude mass yield was 91.5 % at 0 min and 87.8 % at 30 min. The difference between the expected 100 % and the recorded 91.5 % at 0 min is likely due to an incomplete recovery of triolein during the work-up, as confirmed by the blank experiment (Table S1). Conversely, the 87.8 % observed at 30 min represents 96.0 % of the biocrude yield at 0 min, closely aligning with the theoretically expected 95.7 % reduction., This alignment suggests that hydrolysis primarily occurred after 30 min at 325 °C. This assumption was confirmed by the assessment of the hydrolysis yield (Fig. S3), according to Equation (2). This equation is analogous to the glycerol yield, and its application is substantiated by an experimental test involving glycerol alone, which demonstrated that after 30 min at 325 °C, 97 % of glycerol remains unconverted. The hydrolysis yield was minimal at 0 min (0–1.4 %), but almost complete at 30 min (87–90 %). Based on these results, it is reasonable to assume that the kinetics of triglycerides are slow enough that significant hydrolysis does not occur during the initial heating phase, eliminating the influence of heating rate on the final product distribution.

$$Hydrolysis\ yield(\%) = \frac{glycerol\ concentration\ in\ the\ AP \left(\frac{g_{glycerol}}{g_{AP}}\right) \cdot 7.2\ g_{AP}}{0.104 \left(\frac{g_{glycerol}}{g_{triolein}}\right) \cdot 1.8\ g_{triolein}} \quad (2)$$

3.4. Food waste

The biochemical composition of the food waste collected from the university canteen was 19.6 ± 0.7 % proteins, 2.9 ± 1.2 % lipids and 77.5 ± 1.9 % carbohydrates on a dry ash-free basis. A synthetic mixture of cellulose, albumin and triolein was used to mimic the food waste during the HTL reaction, referred to as 'simulated food waste' hereafter. The resulting mass yields are reported in Fig. 5-A, while the linear combination of the mass yields obtained from the singular biopolymers was calculated using Eq. 3, and the results are presented in Fig. 5-B. Interestingly, the linear combination of the mass yields strongly differs with the actual results obtained from the simulated food waste. To further highlight the discrepancies, in Fig. S4-A/B, the absolute and relative differences between the experimental results and the averaged values are plotted. At 0 min and 115 K/min, the solid produced from the simulated food waste significantly exceeded the averaged value. With increasing KSFs, this difference decreased until it was inverted at higher values. The biocrude yield showed an opposite trend, as it was slightly unfavored at low KSFs and ended up being slightly favored at higher KSFs. The differences between the simulated food waste and the linear combination of the biopolymers reacting alone must be explained by synergistic/antagonistic behaviors between the biopolymers. The strongest interaction between biochemical compounds during HTL takes place between carbohydrates and proteins (Lu et al., 2018). As already observed in another work, this interaction leads to an increased production of solid phase at low temperature (KSFs of 4.8 and 6.3 at 200 °C and 250 °C) due to the formation of melanoidin-like compounds that at higher temperatures (KSFs of 7.8 and 9.3 at 300 °C and 350 °C) are converted into biocrude (Tito et al., 2023a). Due to the similar trends observed in this work with biocrude and solid with increasing KSF, the synergistic/antagonistic behavior is likely explained by the presence of the Maillard reaction. Moreover, also the gas yield was increased in the case of the simulated food waste (Fig. S4-A/B). This can be explained by the presence of the Strecker degradation that, during the Maillard reaction, leads to the production of carbon dioxide already at low temperatures (Fang and Schmidt-Rohr, 2009; Tito et al., 2023a; Yaylayan, 2003). Interestingly, the minimal change in biocrude yield observed in simulated food waste after alterations in heating rates with short residence times (Fig. 5-A) can be attributed to this interaction between carbohydrates and proteins. This interaction, as opposed to the linear combination, promotes biocrude production at the cost of solid yield at lower KSF (higher heating rate), while the reverse occurs at higher KSF (lower heating rate).

The mass yields obtained from the HTL experiments with real food waste are reported in Fig. 5-C. The mass yields obtained at 30 min after the HTL of real food waste (Fig. 5-C) were relatively similar to those obtained after the HTL of simulated biomass (Fig. 5-A). Any minor differences could be attributed to the structural distinctions between the constituents of real biomass and the model macromolecules used to mimic it (cellulose, albumin and triolein). However, the trend of the solid phase with varying heating rate significantly differed at 0 min. Specifically, the mass yield decreased with decreasing heating rates in the case of simulated food waste but increased with actual food waste. Before the reaction, both actual and simulated food waste consisted mainly of the solid phase (87 % and 79 %, respectively, as reported in Table S1), which is converted over time. Simultaneously, another solid phase is produced as a result of interactions between molecules in the other phases, such as the formation of insoluble melanoidins (Tito et al., 2023a). Consequently, the resulting solid yield is the outcome of a balance between the conversion of solid food waste and the production of solid intermediates. Therefore, the disparities between real and simulated food waste may arise from the different kinetics of hydrolysis and intermediate formation, which tend to minimize over longer reaction times. The solid phase decreased after increasing the reaction time from 0 to 30 min, while biocrude increased (Fig. 5-C). This trend confirmed the instability of the intermediate solid at higher temperatures and suggests its conversion into biocrude.

It is important to note that the biocrude yield slightly decreased with a decreasing heating rate, even at 30 min. The same trend at 30 min was observed during the HTL of cellulose (Fig. 1), along with an increase in the solid. Although the increase in the solid phase is not clearly visible in Fig. 5, it is likely that the heating rate has a subtle effect on the performances of carbohydrate-containing feedstock, even at higher residence times.

It is worth noting that the biocrude yields reported herein from actual food waste were lower than those reported in the literature (Aierzhati et al., 2019; Motavaf and Savage, 2021). For example, Motavaf and Savage obtained approximately a 28 % yield with similar operating conditions of pressure, temperature and residence time (Motavaf and Savage, 2021). This difference could be explained by the fact that the lipid content of the food waste used as feedstock in this work was extremely low (2.9 $\%_{daf}$ vs 16.6 $\%_{daf}$). Indeed, the biochemical composition of food waste strongly influences the HTL performance, and a higher lipid content translates to a higher biocrude production (Aierzhati et al., 2019). This is corroborated by works performed with similar biochemical content to the one used herein, obtaining

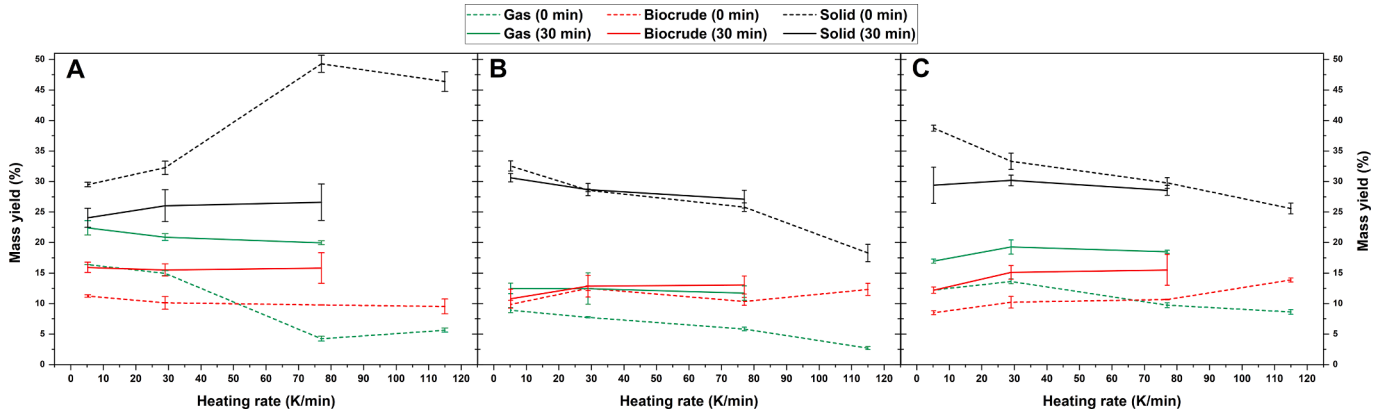

Fig. 5. (A) Mass yields obtained from the simulated food waste. Reaction conditions: 1.36 g cellulose, 0.39 g albumin, 0.05 g triolein, 9 g total, 325 °C, 0 and 30 min. (B) Mass yields obtained as linear combination of cellulose, albumin and triolein reacting alone, evaluated according to Eq. 3. (C) Mass yields obtained from the real food waste. Reaction conditions: 5.6 g food waste (1.8 g dry based), 9 g total, 325 °C, 0 and 30 min.

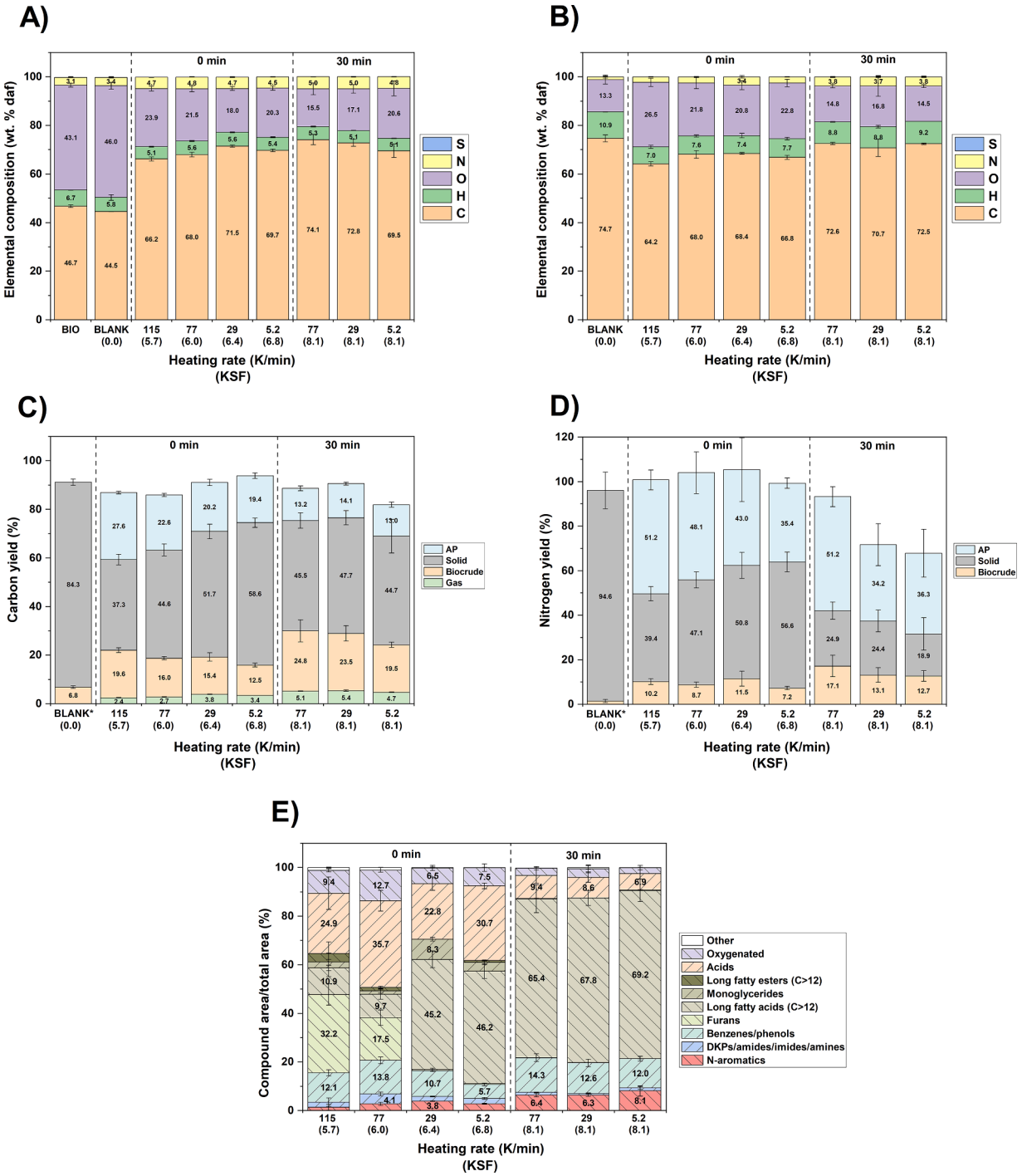

Fig. 6. (A) Elemental composition of solids, feedstock (BIO) and its solid fraction (BLANK); (B) elemental composition of biocrudes and the oil fraction of the feedstock (BLANK); (C) carbon yields of all the phases and of fraction of the feedstock (BLANK); (D) nitrogen yields of all the phases and of fraction of the feedstock (BLANK); (E) families of compounds identified in the biocrudes. Data refer to products obtained from real food waste at 325 °C with different heating rates and with two residence times (0 min, 30 min). *AP not quantified.

comparable values (Aierzhati et al., 2019).

$$Yield_{averaged}\,(\%) = \frac{yield_{cell,dry}\cdot mass_{cell,dry} + yield_{alb,dry}\cdot mass_{alb,dry} + yield_{triol,dry}\cdot mass_{triol,dry}}{mass_{cell,dry} + mass_{alb,dry} + mass_{triol,dry}} \quad (3)$$

Fig. 6-A/B depict the elemental composition of solids and biocrudes, respectively. Even at 0 min and 115 K/min, the elemental compositions of the solid and the biocrude were similar to those obtained after 30 min of reaction time. In the case of solids, carbon ranged within 66–74 %, hydrogen within 5.1–5.6 %, oxygen within 16–24 % and nitrogen within 4.5–5.0 %. Similarly, for biocrudes, carbon ranged within 64–73 %, hydrogen within 7.0–9.2 %, oxygen within 15–27 % and nitrogen within 2.2–3.8 %. For both solids and biocrudes, at 0 min, the carbon content increased with decreasing rate, at the expense of oxygen. In contrast, at 30 min, the elemental composition of the biocrudes did not vary significantly, while the solids decreased the carbon content in favor of oxygen with decreasing heating rate.

-C/D depict the carbon and nitrogen yields in the different phases, respectively. While the carbon and nitrogen were initially exclusively present in the solid fraction of the food waste, after the reaction, both the carbon and nitrogen content increased at 0 min with decreasing heating rate. However, at 30 min, these values decreased compared to those obtained at 0 min, coherently with the mass yields of Fig. 5. On the other hand, biocrudes increased their nitrogen and carbon content as the reaction time increased from 0 to 30 min. Moreover, the carbon yield in the biocrude exhibited a decreasing trend at 30 min with decreasing heating rate, confirming a certain effect of the heating rate even with the same KSFs. As for the AP, the carbon yield decreased from 28 % to 19 % with decreasing heating rate at 0 min, and equaled 13–14 % at 30 min. On the other hand, nitrogen showed a higher distribution in the AP (36–52 %). This aqueous phase can then be further valorized through other technologies (Srivastava et al., 2022b, 2022a; Tito et al., 2023b; Zoppi et al., 2023).

Fig. 6E presents the most prevalent families of molecules identified by GC–MS in the biocrudes, with the highest peaks detailed in Table S5. At 0 min and 115 K/min, the majority of the identified molecules were furans, followed by organic acids, aromatics (benzenes/phenols), long fatty acids, and oxygenated compounds. Apart from fatty acids, this composition closely resembled the biocrude obtained from pure cellulose (Fig. 2-D), coherently with the carbohydrate-rich composition of the food waste. The presence of long fatty acids is attributable to the lipids present in the food waste. While GC–MS cannot identify triglycerides due to their high boiling point, it can detect fatty acids. Consequently, at 0 min with a decreasing heating rate, the content of long fatty acids increased in the GC–MS, eventually constituting the majority of the integrated area at 30 min. This increase is the result of the hydrolysis of fatty acids, as observed with triolein (Fig. S3). However, only the vaporized fraction of the biocrude is analyzed with GC–MS. Fig. S5 illustrates that approximately 48 % of the biocrude evaporates prior to reaching 280 °C, which is the injection temperature of the GC–MS. Consequently, the composition depicted in -E solely represents this 48 %. This observation may elucidate why Fig. 6-E indicates that 68 % of the biocrude consists of fatty acids, particularly when considering that, at the 30-minute mark, about 15 wt% of the biocrude was generated, while the biomass waste contained only 3 wt% of lipids. In addition to long fatty acids, monoglycerides and long fatty esters were detected, particularly at 0 min, as products of the partial hydrolysis of triglycerides and degradation of monoglycerides (Gollakota and Savage, 2018).

By excluding the area attributed to long fatty acids, the area associated with furans decreased as the heating rate decreased at 0 min. In its place, we observed an increase in the presence of acids, phenols, and nitrogen-containing aromatics, ultimately becoming the three most abundant compound families after 30 min of the reactions. The significant presence of acids and phenols aligns with the carbohydrate-rich content, while the presence of nitrogen-containing aromatics is due to the proteinaceous content of the food waste. Notably, in contrast to the composition of the biocrude derived from albumin, this case revealed that pyridines, rather than indoles, constituted the majority of the nitrogen-containing aromatics, suggesting a different mechanism of formation (Inoue et al., 2004). Furthermore, the GC–MS results for the simulated food (Fig. S6) closely resembled those of -E, indicating a chemical resemblance between biocrude from real waste and model macromolecules.

4. General considerations

With the exception of triolein, which requires high temperatures for hydrolysis, cellulose, albumin, real and simulated food waste showed significant variations in performance when the heating rate was changed at 0 min. These differences were both quantitative (e.g., mass, carbon and nitrogen yields) and qualitative (e.g., biocrude composition). This behavior can be explained by an 'indirect' effect of the heating rate on reaction kinetics, represented by the KSF. Specifically, at short reaction times, decreases in the heating rate lead to increases in the heating time, resulting in a higher KSF and hence a higher advancement of the reaction. Conversely, after an additional 30 min at the set-point temperature, the differences in both quantitative and qualitative aspects resulting from variations in the heating rate became less evident. Because of this, it can be assumed that any 'direct' effects during the heating time - associated to the fact that a prolonged permanence at lower temperatures during heating time could induce changes in mechanisms and, consequently, overall selectivity - are limited. Therefore, the primary effect associated with the heating rate is kinetic, and any intermediate produced at different heating rates converts into the same product when the time at the set-point temperature is extended.

To further reinforce this concept, Fig. S7 plots biocrude and solid yield against the KSF. With short reaction times (KSF < 7), some trends of the mass yields were clearly visible with the KSF. Conversely, for the experiments lasting 30 min, having the same KSF of 8.1, the mass yields were similar. Notably, some differences outside the standard deviations arose for solid in the case of cellulose and for biocrude in the case of cellulose and food waste. In those cases, biocrude production was favored at the expense of solid when using faster heating rates. Nevertheless, in contrast to the variances noted with diverse KSFs, these distinctions were negligible. Additionally, while there were slight variations in yields for these two types of feedstocks under different heating rates, there were no qualitative changes observed in the composition of the biocrude, as depicted in Fig. 2-D, Fig. 4-F and -E.

5. Conclusions

In this study, the heating rate's impact on HTL of food waste and model compounds was investigated. Higher heating rates at shorter reaction times resulted in significant changes: solid yield declined (-34 %), biocrude yield rose (+63 %), and its composition changed with food waste. Conversely, limited effects were observed at longer reaction times. The heating rate impact was attributed to change in the kinetic

advancement of the reaction, while minor differences were attributed to direct influences on reaction mechanisms. The kinetic severity factor proved useful in considering the heating rate in relation to temperature and operating time. The study emphasizes heating rate's crucial role in fast HTL, with limited impact in isothermal conditions.

CRediT authorship contribution statement

Edoardo Tito: Writing – review & editing, Writing – original draft, Methodology, Formal analysis, Data curation, Conceptualization. **Carlo Alberto Marcolongo:** Methodology, Investigation, Data curation. **Giuseppe Pipitone:** Writing – review & editing, Validation, Supervision, Methodology, Data curation, Conceptualization. **Alessandro H.A. Monteverde:** Validation, Supervision. **Samir Bensaid:** Validation, Supervision, Project administration, Conceptualization. **Raffaele Pirone:** Writing – review & editing, Validation, Supervision, Project administration, Funding acquisition, Conceptualization.

Declaration of competing interest

The authors declare that they have no known competing financial interests or personal relationships that could have appeared to influence the work reported in this paper.

Data availability

The data that support the findings of this study are available from the corresponding author upon reasonable request.

Acknowledgment

This study was carried out within the ReFuel project – funded by European Union – Next Generation EU within the PRIN 2022 program (D.D. 104 - 02/02/2022 Ministero dell'Università e della Ricerca). This manuscript reflects only the authors' views and opinions and the Ministry cannot be considered responsible for them.

Appendix A. Supplementary data

Supplementary data to this article can be found online at https://doi.org/10.1016/j.biortech.2024.130446.

Bibliography

Aida, T.M., Oshima, M., Smith, R.L., 2017. Controlled conversion of proteins into high-molecular-weight peptides without additives with high-temperature water and fast heating rates. ACS Sustain. Chem. Eng. 5, 7709–7715. https://doi.org/10.1021/acssuschemeng.7b01146.

Aierzhati, A., Stablein, M.J., Wu, N.E., Kuo, C.T., Si, B., Kang, X., Zhang, Y., 2019. Experimental and model enhancement of food waste hydrothermal liquefaction with combined effects of biochemical composition and reaction conditions. Bioresour. Technol. 284, 139–147. https://doi.org/10.1016/j.biortech.2019.03.076.

Bach, Q.-V., Sillero, M.V., Tran, K.-Q., Skjermo, J., 2014. Fast hydrothermal liquefaction of a norwegian macro-alga: screening tests. Algal Res. 6, 271–276. https://doi.org/10.1016/j.algal.2014.05.009.

Biller, P., Ross, A.B., 2011. Potential yields and properties of oil from the hydrothermal liquefaction of microalgae with different biochemical content. Bioresour. Technol. 102, 215–225. https://doi.org/10.1016/j.biortech.2010.06.028.

Brand, S., Hardi, F., Kim, J., Suh, D.J., 2014. Effect of heating rate on biomass liquefaction: differences between subcritical water and supercritical ethanol. Energy 68, 420–427. https://doi.org/10.1016/j.energy.2014.02.086.

Castello, D., Pedersen, T., Rosendahl, L., 2018. Continuous hydrothermal liquefaction of biomass: a critical review. Energies 11, 3165. https://doi.org/10.3390/en11113165.

Changi, S.M., Faeth, J.L., Mo, N., Savage, P.E., 2015. Hydrothermal reactions of biomolecules relevant for microalgae liquefaction. Ind. Eng. Chem. Res. 54, 11733–11758. https://doi.org/10.1021/acs.iecr.5b02771.

Chay Pak Ting, B.P., Pouliot, Y., Gauthier, S.F., Mine, Y., 2013. Fractionation of egg proteins and peptides for nutraceutical applications, in: Separation, Extraction and Concentration Processes in the Food, Beverage and Nutraceutical Industries. Elsevier, pp. 595–618. https://doi.org/10.1533/9780857090751.2.595.

Chen, W.-H., Lin, Y.-Y., Liu, H.-C., Baroutian, S., 2020. Optimization of food waste hydrothermal liquefaction by a two-step process in association with a double analysis. Energy 199, 117438. https://doi.org/10.1016/j.energy.2020.117438.

Cheng, F., Cui, Z., Mallick, K., Nirmalakhandan, N., Brewer, C.E., 2018. Hydrothermal liquefaction of high- and low-lipid algae: mass and energy balances. Bioresour. Technol. 258, 158–167. https://doi.org/10.1016/j.biortech.2018.02.100.

Chum, H.L., Johnson, D.K., Black, S.K., Overend, R.P., 1990. Pretreatment-catalyst effects and the combined severity parameter. Appl. Biochem. Biotechnol. 24–25, 1–14. https://doi.org/10.1007/BF02920229.

Déniel, M., Haarlemmer, G., Roubaud, A., Weiss-Hortala, E., Fages, J., 2016. Energy valorisation of food processing residues and model compounds by hydrothermal liquefaction. Renew. Sustain. Energy Rev. 54, 1632–1652. https://doi.org/10.1016/j.rser.2015.10.017.

Déniel, M., Haarlemmer, G., Roubaud, A., Weiss-Hortala, E., Fages, J., 2017. Hydrothermal liquefaction of blackcurrant pomace and model molecules: understanding of reaction mechanisms. Sustain. Energy Fuels 1, 555–582. https://doi.org/10.1039/C6SE00065G.

Dote, Y., Inoue, S., Ogi, T., Yokoyama, S.Y., 1998. Distribution of nitrogen to oil products from liquefaction of amino acids. Bioresour. Technol. 64, 157–160. https://doi.org/10.1016/S0960-8524(97)00079-5.

Faeth, J.L., Valdez, P.J., Savage, P.E., 2013. Fast hydrothermal liquefaction of nannochloropsis sp. to produce biocrude. Energy and Fuels 27, 1391–1398. https://doi.org/10.1021/ef301925d.

Fan, Q., Fu, P., Song, C., Fan, Y., 2023. Valorization of waste biomass through hydrothermal liquefaction: a review with focus on linking hydrothermal factors to products characteristics. Ind. Crops Prod. 191, 116017 https://doi.org/10.1016/j.indcrop.2022.116017.

Fang, X., Schmidt-Rohr, K., 2009. Fate of the amino acid in glucose-glycine melanoidins investigated by solid-state nuclear magnetic resonance (NMR). J. Agric. Food Chem. 57, 10701–10711. https://doi.org/10.1021/jf9020587.

FAO, 2011. Global food losses and food waste-Extent, causes and prevention. Rome.

FAO, 2013. Reducing the Food Wastage Footprint (Toolkit). Rome.

FAO, 2019. The State of Food and Agriculture. Rome.

Gollakota, A.R.K., Kishore, N., Gu, S., 2018. A review on hydrothermal liquefaction of biomass. Renew. Sustain. Energy Rev. 81, 1378–1392. https://doi.org/10.1016/j.rser.2017.05.178.

Gollakota, A., Savage, P.E., 2018. Hydrothermal liquefaction of model food waste biomolecules and ternary mixtures under isothermal and fast conditions. ACS Sustain. Chem. Eng. 6, 9018–9027. https://doi.org/10.1021/acssuschemeng.8b01368.

Hietala, D.C., Faeth, J.L., Savage, P.E., 2016. A quantitative kinetic model for the fast and isothermal hydrothermal liquefaction of nannochloropsis sp. Bioresour. Technol. 214, 102–111. https://doi.org/10.1016/j.biortech.2016.04.067.

Inoue, S., Noguchi, M., Hanaoka, T., Minowa, T., 2004. Organic compounds formed by thermochemical degradation of glucose-glycine melanoidins using hot compressed water. J. Chem. Eng. Japan 37, 915–919. https://doi.org/10.1252/jcej.37.915.

Jakob, A., Grilc, M., Teržan, J., Likozar, B., 2021. Solubility temperature dependence of bio-based levulinic acid, furfural, and hydroxymethylfurfural in water, nonpolar. Polar Aprotic and Protic Solvents. Processes 9, 924. https://doi.org/10.3390/pr9060924.

Kamio, E., Takahashi, S., Noda, H., Fukuhara, C., Okamura, T., 2008. Effect of heating rate on liquefaction of cellulose by hot compressed water. Chem. Eng. J. 137, 328–338. https://doi.org/10.1016/j.cej.2007.05.007.

Kumar, R., 2022. A review on the modelling of hydrothermal liquefaction of biomass and waste feedstocks. Energy Nexus 5, 100042. https://doi.org/10.1016/j.nexus.2022.100042.

Lu, J., Liu, Z., Zhang, Y., Savage, P.E., 2018. Synergistic and antagonistic interactions during hydrothermal liquefaction of soybean oil, soy protein, cellulose, xylose, and lignin. ACS Sustain. Chem. Eng. 6, 14501–14509. https://doi.org/10.1021/acssuschemeng.8b03156.

Madsen, R.B., Zhang, H., Biller, P., Goldstein, A.H., Glasius, M., 2017. Characterizing semivolatile organic compounds of biocrude from hydrothermal liquefaction of biomass. Energy and Fuels 31, 4122–4134. https://doi.org/10.1021/acs.energyfuels.7b00160.

Mahadevan Subramanya, S., Savage, P.E., 2021. Identifying and modeling interactions between biomass components during hydrothermal liquefaction in sub-, near-, and supercritical water. ACS Sustain. Chem. Eng. 9, 13874–13882. https://doi.org/10.1021/acssuschemeng.1c04810.

Mathanker, A., Das, S., Pudasainee, D., Khan, M., Kumar, A., Gupta, R., 2021. A review of hydrothermal liquefaction of biomass for biofuels production with a special focus on the effect of process parameters, co-solvents and extraction solvents. Energies 14, 4916. https://doi.org/10.3390/en14164916.

Mathimani, T., Mallick, N., 2019. A review on the hydrothermal processing of microalgal biomass to bio-oil - knowledge gaps and recent advances. J. Clean. Prod. 217, 69–84. https://doi.org/10.1016/j.jclepro.2019.01.129.

Mishra, R.K., Kumar, V., Kumar, P., Mohanty, K., 2022. Hydrothermal liquefaction of biomass for bio-crude production: a review on feedstocks, chemical compositions, operating parameters, reaction kinetics, techno-economic study, and life cycle assessment. Fuel 316, 123377. https://doi.org/10.1016/j.fuel.2022.123377.

Motavaf, B., Savage, P.E., 2021. Effect of process variables on food waste valorization via hydrothermal liquefaction. ACS ES&T Eng. 1, 363–374. https://doi.org/10.1021/acsestengg.0c00115.

Overend, R.P., Chornet, E., 1987. Fractionation of lignocellulosics by steam-aqueous pretreatments. philos. trans. R. Soc. London. ser. a. Math. Phys. Sci. 321, 523–536. https://doi.org/10.1098/rsta.1987.0029.

Prestigiacomo, C., Laudicina, V.A., Siragusa, A., Scialdone, O., Galia, A., 2020. Hydrothermal liquefaction of waste biomass in stirred reactors: one step forward to the integral valorization of municipal sludge. Energy 201, 117606. https://doi.org/10.1016/j.energy.2020.117606.

Prestigiacomo, C., Scialdone, O., Galia, A., 2022. Hydrothermal liquefaction of wet biomass in batch reactors: critical assessment of the role of operating parameters as a function of the nature of the feedstock. J. Supercrit. Fluids. https://doi.org/10.1016/j.supflu.2022.105689.

Qian, L., Wang, S., Savage, P.E., 2020. Fast and isothermal hydrothermal liquefaction of sludge at different severities: reaction products, pathways, and kinetics. Appl. Energy 260, 114312. https://doi.org/10.1016/j.apenergy.2019.114312.

Qiu, Y., Aierzhati, A., Cheng, J., Guo, H., Yang, W., Zhang, Y., 2019. Biocrude oil production through the maillard reaction between leucine and glucose during hydrothermal liquefaction. Energy and Fuels 33, 8758–8765. https://doi.org/10.1021/acs.energyfuels.9b01875.

Rasmussen, H., Sørensen, H.R., Meyer, A.S., 2014. Formation of degradation compounds from lignocellulosic biomass in the biorefinery: sugar reaction mechanisms. Carbohydr. Res. 385, 45–57. https://doi.org/10.1016/j.carres.2013.08.029.

Ruiz, H.A., Rodríguez-Jasso, R.M., Fernandes, B.D., Vicente, A.A., Teixeira, J.A., 2013. Hydrothermal processing, as an alternative for upgrading agriculture residues and marine biomass according to the biorefinery concept: a review. Renew. Sustain. Energy Rev. 21, 35–51. https://doi.org/10.1016/j.rser.2012.11.069.

Sakata, K., Kitadai, N., Yokoyama, T., 2010. Effects of pH and temperature on dimerization rate of glycine: evaluation of favorable environmental conditions for chemical evolution of life. Geochim. Cosmochim. Acta 74, 6841–6851. https://doi.org/10.1016/j.gca.2010.08.032.

Sasaki, M., Kabyemela, B., Malaluan, R., Hirose, S., Takeda, N., Adschiri, T., Arai, K., 1998. Cellulose hydrolysis in subcritical and supercritical water. J. Supercrit. Fluids 13, 261–268. https://doi.org/10.1016/S0896-8446(98)00060-6.

Sheehan, J.D., Savage, P.E., 2017. Molecular and lumped products from hydrothermal liquefaction of bovine serum albumin. ACS Sustain. Chem. Eng. 5, 10967–10975. https://doi.org/10.1021/acssuschemeng.7b02854.

Simonne, A.H., Simonne, E.H., Eitenmiller, R.R., Mills, H.A., Cresman, C.P., 1997. Could the dumas method replace the kjeldahl digestion for nitrogen and crude protein determinations in foods? J. Sci. Food Agric. 73, 39–45. https://doi.org/10.1002/(SICI)1097-0010(199701)73:1<39::AID-JSFA717>3.3.CO;2-W.

Srivastava, R.K., Boddula, R., Pothu, R., 2022a. Microbial fuel cells: technologically advanced devices and approach for sustainable/renewable energy development. Energy Convers. Manag. X 13, 100160. https://doi.org/10.1016/j.ecmx.2021.100160.

Srivastava, R.K., Pothu, R., Sanchez, C.P., Goswami, T., Mitra, S., Rene, E.R., Nedungadi, S.V., 2022b. Removal and recovery of nutrients and value-added products from wastewater: technological options and practical perspective. Syst. Microbiol. Biomanufacturing 2, 67–90. https://doi.org/10.1007/s43393-021-00056-6.

Teri, G., Luo, L., Savage, P.E., 2014. Hydrothermal treatment of protein, polysaccharide, and lipids alone and in mixtures. Energy and Fuels 28, 7501–7509. https://doi.org/10.1021/ef501760d.

Tito, E., Pipitone, G., Monteverde Videla, A.H.A., Bensaid, S., Pirone, R., 2023a. Exploring HTL pathways in carbohydrate–protein mixture: a study on glucose–glycine interaction. Biomass Convers. Biorefinery 13, 16385–16404. https://doi.org/10.1007/s13399-023-03967-7.

Tito, E., Zoppi, G., Pipitone, G., Miliotti, E., Fraia, A.D., Rizzo, A.M., Pirone, R., Chiaramonti, D., Bensaid, S., 2023b. Conceptual design and techno-economic assessment of coupled hydrothermal liquefaction and aqueous phase reforming of lignocellulosic residues. J. Environ. Chem. Eng. 11, 109076 https://doi.org/10.1016/j.jece.2022.109076.

Toor, S.S., Rosendahl, L., Rudolf, A., Sohail, S., Rosendahl, L., Rudolf, A., 2011. Hydrothermal liquefaction of biomass: a review of subcritical water technologies. Energy 36, 2328–2342. https://doi.org/10.1016/j.energy.2011.03.013.

Torri, C., Garcia Alba, L., Samorì, C., Fabbri, D., Brilman, D.W.F., 2012. Hydrothermal treatment (HTT) of microalgae: detailed molecular characterization of HTT oil in view of HTT mechanism elucidation. Energy and Fuels 26, 658–671. https://doi.org/10.1021/ef201417e.

Tran, K.-Q., Klemsdal, A.J., Zhang, W., Sandquist, J., Wang, L., Skreiberg, Ø., 2017. Fast hydrothermal liquefaction of native and torrefied wood. Energy Procedia 105, 218–223. https://doi.org/10.1016/j.egypro.2017.03.305.

Velasco Calderón, J.C., Arora, J.S., Mushrif, S.H., 2022. Mechanistic investigation into the formation of humins in acid-catalyzed biomass reactions. ACS Omega 7, 44786–44795. https://doi.org/10.1021/acsomega.2c04783.

Yang, J., He, Q., (Sophia), Corscadden, K., Niu, H., Lin, J., Astatkie, T., 2019. Advanced models for the prediction of product yield in hydrothermal liquefaction via a mixture design of biomass model components coupled with process variables. Appl. Energy 233–234, 906–915. https://doi.org/10.1016/j.apenergy.2018.10.035.

Yaylayan, V.A., 2003. Recent advances in the chemistry of strecker degradation and amadori rearrangement: implications to aroma and color formation. Nippon Shokuhin Kagaku Kogaku Kaishi 50, 372–377. https://doi.org/10.3136/nskkk.50.372.

Zhang, C., Tang, X., Sheng, L., Yang, X., 2016. Enhancing the performance of co-hydrothermal liquefaction for mixed algae strains by the maillard reaction. Green Chem. 18, 2542–2553. https://doi.org/10.1039/C5GC02953H.

Zoppi, G., Andrade, T.A., Ward, A.J., Ambye-Jensen, M., Biller, P., 2023. Biorefinery integration of a green protein platform for maximum resource utilization. Clean. Circ. Bioeconomy 6, 100064. https://doi.org/10.1016/j.clcb.2023.100064.